

Combining Hyperspectral and Lidar Data for Vegetation Mapping in the Florida Everglades

Caiyun Zhang

Abstract

This study explored a combination of hyperspectral and lidar systems for vegetation mapping in the Florida Everglades. A framework was designed to integrate two remotely sensed datasets and four data processing techniques. Lidar elevation and intensity features were extracted from the original point cloud data to avoid the errors and uncertainties in the raster-based lidar methods. Lidar significantly increased the classification accuracy compared with the application of hyperspectral data alone. Three lidar-derived features (elevation, intensity, and topography) had the same contributions in the classification. A synergy of hyperspectral imagery with all lidar-derived features achieved the best result with an overall accuracy of 86 percent and a Kappa value of 0.82 based on an ensemble analysis of three machine learning classifiers. Ensemble analysis did not significantly increase the classification accuracy, but it provided a complementary uncertainty map for the final classified map. The study shows the promise of the synergy of hyperspectral and lidar systems for mapping complex wetlands.

Introduction

The Importance of Vegetation Information in the Florida Everglades

The Florida Everglades is the largest subtropical wetland in the United States. It has been designated as an International Biosphere Reserve, a World Heritage Site, and a Wetland of International Importance due to its unique combination of hydrology and water-based ecology that supports many threatened and endangered species (Davis *et al.*, 1994). In the past century, human activities have severely modified the Everglades ecosystem, resulting in a variety of environmental issues in South Florida (McPherson and Halley, 1996). To protect this valuable resource the US Congress authorized the Comprehensive Everglades Restoration Plan (CERP) in 2000 to restore the Everglades ecosystem (CERP, 2013). CERP is a \$10.5 billion USD mission that is expected to take 30 or more years to complete. It contains a variety of pilot environmental engineering projects, many of which require accurate and informative vegetation maps, because the restoration will cause dramatic modification of plant communities (Doren *et al.*, 1999). Monitoring changes of vegetation communities can measure the progress and effects of restoration on environmental health (Doren *et al.*, 1999; Welch *et al.*, 1999).

Vegetation Mapping Using Hyperspectral and Lidar Systems

Vegetation mapping efforts to support CERP have focused on manual interpretation of large-scale aerial photographs using analytical stereo plotters (Rutchey *et al.*, 2008; Jones, 2011). This procedure is time-consuming and labor-intensive. Automated classification of the digital aerial photograph cannot

produce the requisite accuracy due to its poor spectral resolution (Zhang and Xie, 2013b). Two promising remote sensing techniques, hyperspectral and the Light Detection And Ranging (lidar) systems, offer significant advantages over manual interpretation of aerial photographs.

Hyperspectral sensors collect data in hundreds of relatively narrow spectral bands throughout the visible and infrared portions of the electromagnetic spectrum. Research has demonstrated the merit of hyperspectral data in a range of applications such as quantifying agricultural crops, classifying vegetation types, and characterizing wetlands (Thenkabail *et al.*, 2011). The application of hyperspectral systems has become an important area of research for wetland mapping in the past decade (Adam *et al.*, 2010). Such research can be grouped into two categories. The first is the employment of hyperspectral data alone (e.g., Hunter and Power, 2002; Hirano *et al.*, 2003; Schmidt *et al.*, 2004; Artigas and Yang, 2005; Harken and Sugumaran, 2005; Li *et al.*, 2005; Rosso *et al.*, 2005; Pengra *et al.*, 2007; Jollineau and Howarth, 2008; Zhang and Xie, 2012; Zhang and Xie, 2013a). The second is the application of a synergy of hyperspectral and other remote sensing data for a better characterization of wetlands (e.g., Held *et al.*, 2003; Yang and Artigas, 2010; Onojeghuo and Blackburn, 2011; Zhang and Xie, 2013b).

Lidar systems were originally designed to facilitate the collection of data for digital terrain modeling by using the reflections from the ground. Studies have illustrated that lidar can be used to characterize vegetation, especially forests, using non-ground reflections (Hyypä *et al.*, 2008; van Leeuwen and Nieuwenhuis, 2010). Lidar can complement the spectral information of optical imagery to improve vegetation classification. Encouraging results have been achieved by integrating lidar data and hyperspectral imagery (e.g., Hill and Thomson, 2005; Mundt *et al.*, 2006; Geerling *et al.*, 2007; Jones *et al.*, 2010; Onojeghuo and Blackburn, 2011; Zhang and Qiu, 2012; Cho *et al.*, 2012). Research efforts on vegetation characterization using lidar is dominated by high-posting-density (i.e., >4 pts/m²) lidar data (Ke *et al.*, 2010; Zhang *et al.*, 2013). Application of low-posting-density (i.e., <2 pts/m²) lidar focuses on terrestrial topographic mapping, and its research in vegetation mapping is limited (Ke *et al.*, 2010). Little work has been conducted to combine low-posting-density lidar data with hyperspectral imagery for vegetation mapping in the complex wetlands. In addition, most lidar vegetation studies have only examined the contribution of elevation information. Few studies have explored the combined contribution of all the

Photogrammetric Engineering & Remote Sensing
Vol. 80, No. 8, August 2014, pp. 000–000.
0099-1112/14/8008–000

© 2014 American Society for Photogrammetry
and Remote Sensing
doi: 10.14358/PERS.80.8.000

Department of Geosciences, Florida Atlantic University, 777
Glades Road, Florida 33431 (czhang3@fau.edu).

potential information extracted from lidar, which includes elevation, intensity, and topography features, in mapping wetlands (Chust *et al.*, 2008).

Classification Algorithms

Most researchers use endmember-based algorithms to classify hyperspectral imagery for wetland mapping such as the Spectral Angle Mapper (SAM) and linear spectral unmixing (e.g., Hunter and Power, 2002; Held *et al.*, 2003; Hirano *et al.*, 2003; Schmidt *et al.*, 2004; Artigas and Yang, 2005; Harken and Sugumaran, 2005; Li *et al.*, 2005; Rosso *et al.*, 2005; Belluco *et al.*, 2006; Jollineau and Howarth, 2008). These classifiers cannot produce the expected results in complex wetlands due to the difficulties inherent in determining endmembers, a shortage of comprehensive spectral libraries for different wetland plants, and/or the violation of an assumption in the algorithms that only one spectral representative (i.e., the endmember) exists for each vegetation type (Zhang and Xie, 2012). Traditional classifiers such as maximum likelihood and minimum distance also cannot generate high accuracies, because they are not able to characterize the high degree of spatial and spectral heterogeneity of the Everglades even after the dimensionality of hyperspectral data is reduced (Zhang and Xie, 2012).

Contemporary machine learning algorithms such as Random Forest (RF), Support Vector Machines (SVMs), and *k*-Nearest Neighbor (*k*-NN) show promise in processing hyperspectral imagery (Ham *et al.*, 2005; Chan and Paelinckx, 2008; Waske *et al.*, 2009; Mountrakis *et al.*, 2010; Zhang and Xie, 2013a and 2013b). For this study, the performance of RF, SVM, and *k*-NN was evaluated for classifying a fused dataset from hyperspectral imagery and lidar data. The classification results from RF, SVM, and *k*-NN may be different for each class. A combination of the strengths of each classifier may have the potential for a better mapping through ensemble analysis techniques. Thus, classifier ensemble techniques were also evaluated.

Mapping Methods

Pixel-based mapping may lead to a “salt-and-pepper” effect at heterogeneous landscapes. It has been well documented that this issue can be overcome by Object-Based Image Analysis (OBIA) techniques which first decompose an image scene into relatively homogeneous areas and then classify these areas instead of pixels. A review of OBIA for multispectral image analysis can be found in Blaschke (2010). Researchers commonly conduct the pixel-based wetland mapping when hyperspectral imagery was used. Several studies have evaluated OBIA techniques in hyperspectral image analysis and find that they are more useful than pixel-based methods due to the valuable spatial information derived for each object (e.g., Harken and Sugumaran, 2005; Addink *et al.*, 2007; Plaza *et al.*, 2009; Kamal and Phinn, 2011; Zhang and Xie, 2012 and 2013a; Cohen *et al.*, 2013). For this study, the object-based mapping methods were used.

Objectives

Hyperspectral, lidar, data fusion, OBIA, machine learning, and ensemble analysis are popular techniques in remote sensing. However, a combination of them for vegetation characterization is limited. Integration of low-posting-density lidar data and hyperspectral imagery for object-based vegetation mapping in complex wetlands is even scarcer. To this end, the main objectives of this study are: (a) to design a framework to combine two remotely sensed datasets (hyperspectral and lidar data) and four image processing techniques (data fusion, OBIA, machine learning, and ensemble analysis) in the mapping procedure, and (b) to examine the applicability of hyperspectral and lidar systems in mapping complex wetlands such as the Florida Everglades.

Study Area and Data

Study Area

The study site is a portion of the Lake Okeechobee watershed in the central Everglades (Figure 1). Lake Okeechobee is the largest freshwater lake in Florida. It is the heart of the Everglades ecosystem by providing water to the surrounding communities. The lake's health has been threatened in recent decades by excessive nutrients from agricultural and urban activities, harmful high and low water levels, as well as the spread of exotic vegetation (CERP, 2013). Restoration of the Lake Okeechobee watershed and associated plant communities is one of the key components in CERP. The study site covers an area of about 50 km² with 13 common Everglades vegetation communities present: *Unimproved Pastures, Upland Shrub and Brushland, Mixed Rangeland, Upland Hardwood, Brazilian Pepper (exotic species), Live Oak, Upland Mixed Coniferous/Hardwood, Mixed Shrub, Freshwater Marshes/Graminoid Prairie-Marsh, Wet Prairie, Emergent Aquatic Vegetation, Sugar Cane, and Herbaceous (Dry Prairie)*.

Data

Data sources include the hyperspectral imagery, lidar, digital aerial photography, and reference data. Hyperspectral imagery was collected by Airborne Visible/Infrared Imaging Spectrometer (AVIRIS) on 30 May 2002 with a spatial resolution of 12 meters. Data were preprocessed at the Jet Propulsion Laboratory Data Facility of National Aeronautics and Space Administration (NASA) to remove fundamental geometric and radiometric errors before transferring them to users. AVIRIS is a premier instrument in the realm of Earth remote sensing. It delivers calibrated hyperspectral images in 224 contiguous spectral channels with wavelengths between 400 nm to 2500 nm. The South Florida Water Management District (SFWMD), one of the partners in CERP, conducted the AVIRIS survey over the Lake Okeechobee watershed to provide the best possible data for the restoration project.

Lidar data were collected by Merrick & Company using a Leica ALS-50 system in December 2007 to support the Florida Division of Emergency Management. The Leica ALS-50 lidar system collects small footprint multiple returns, and intensity at 1060 nm wavelength. The vendors reported the positional accuracy was 0.015 meters horizontally and 0.06 meters vertically at the 95 percent confidence level. The averaged point density for the study area is 1.18 pts/m². The original lidar point cloud data were processed by the vendor to generate the Digital Terrain Model (DTM) using Merrick Advanced Remote Sensing (MARS) processing software (Merrick & Company, Greenwood Village, Colorado). All the lidar point cloud data and DTM are available to the public at the International Hurricane Research Center (<http://mapping.ihrc.fiu.edu/>).

The SFWMD also provided large scale aerial photography collected in May 2003 and a digital vegetation database for the study site. The vegetation database was built by interpreting the collected aerial photograph in a 3D environment using Kork stereo plotters. Vegetation communities were classified based on the SFWMD modified Florida Land Use, Land Cover Classification System. Note that there is a year gap between the acquisition of the AVIRIS data and the aerial photograph; changes may have occurred during this year. Fortunately, the AVIRIS imagery allows the visual interpretation of vegetation communities with assistance from the database and related aerial photography. A total of 596 image objects were randomly selected and visually interpreted. These objects were used as the reference data in this study. A spatially stratified data sampling strategy was followed in the reference data selection procedure. The number of reference samples for each community was roughly estimated based on the results of image segmentation and the vegetation database. The segmentation

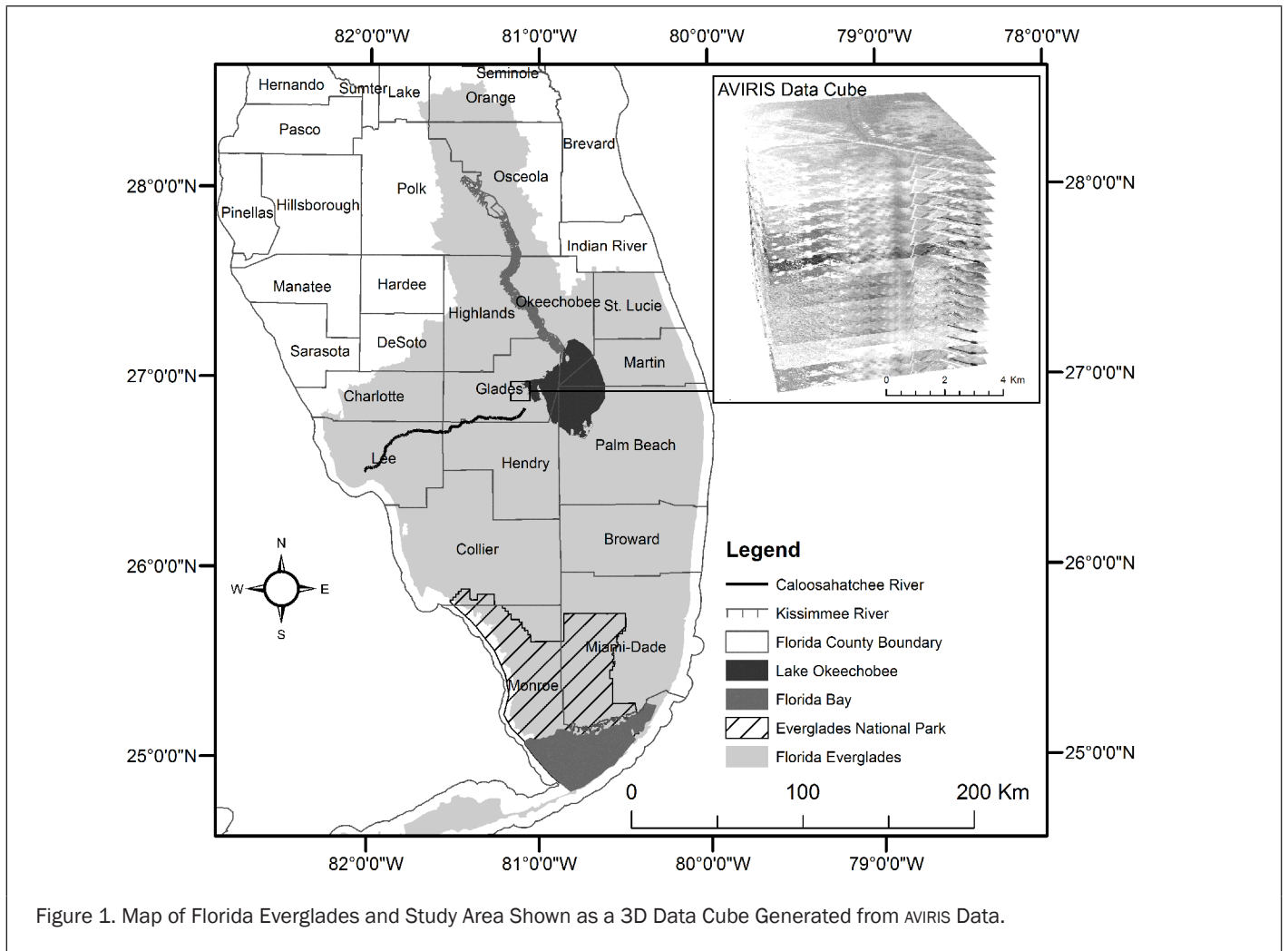


Figure 1. Map of Florida Everglades and Study Area Shown as a 3D Data Cube Generated from AVIRIS Data.

process to generate image objects is detailed in the Methodology section. The reference objects were split into two halves with one for calibration and the other for validation. Non-vegetation objects (i.e., water and levees) were masked out since the main concern of this study was vegetation. Water was discriminated using near infrared and shortwave infrared, while levees were masked out using the digital database.

Methodology

Data Preprocessing

Spectral channels with a low signal-to-noise ratio and strong water absorption were dropped from the AVIRIS imagery, leaving 53 bands (20 visible: 413 nm–692 nm; 24 near-infrared: 702 nm–1263 nm; and 9 shortwave infrared: 1323 nm–1692 nm) for further analysis. This step was conducted by visually examining each individual band in ENVI 4.7. After the noisy band elimination, an image to image registration was employed to georeference the AVIRIS data using the aerial photograph in order to geographically align the AVIRIS data with the digital vegetation database. Radiometric calibration is frequently conducted for hyperspectral datasets if the remote sensing derived reflectance needs to be quantitatively compared with *in situ* spectral reflectance data. It is not generally necessary to perform atmospheric correction for image classification if a single scene is used. As long as the training data from the image to be classified have the same relative scale (corrected or uncorrected), atmospheric correction has little effect on classification (Jensen, 2004). For this study

atmospheric correction of the AVIRIS imagery was unnecessary because firstly no comparison of spectral reflectance from AVIRIS data and *in-situ* data was needed; and secondly only one scene was used in the classification.

Hyperspectral data has a high dimensionality and contains a tremendous amount of redundant spectral information. When the number of spectral channels exceeds a given limit of fixed training samples, the classification accuracy will decrease. This is known as Hughes Phenomenon (or “the curse of high dimensionality”) (Hughes, 1968). To solve this problem in hyperspectral data classification, a number of methods have been developed to reduce the high dimensionality of hyperspectral data. Such methods can be grouped into two categories (Webb, 2002). The first one is to identify spectral channels that do not contribute to the classification and ignore them (known as feature selection), such as the lambda-lambda R^2 model. The second one is to find a transformation from a higher dimensional to a lower dimensional feature space to preserve the most desired information content (known as feature extraction). Examples include Principal Component Analysis (PCA), Independent Component Analysis (ICA), Stepwise Discriminant Analysis (SDA), and Minimum Noise Fraction (MNF) (Zhang *et al.*, 2007). Thenkabail *et al.* (2004 and 2013) have successfully applied the lambda-lambda R^2 models, PCA, and SDA in hyperspectral vegetation analysis. Previous studies have revealed that MNF method not only reduces data dimensionality, but also removes the inherent noise in hyperspectral imagery to improve classification accuracy (Zhang and Xie, 2012; Zhang and Xie, 2013a). Thus

the MNF approach was selected in this study.

The MNF transformation applies two cascaded principal component analyses, with the first transformation decorrelating and rescaling noise in the data, and the second transformation creating coherent eigenimages that contain useful information and generating noise-dominated eigenimages (Green *et al.*, 1988). The transformation generates the eigenvalues and corresponding eigenimages, both of which are used to determine the true dimensionality of the data. The MNF transformation was conducted in ENVI 4.7. The first 10 MNF eigenimages were proved the most useful and spatially coherent and thus selected for further analysis.

A Framework to Combine Hyperspectral and Lidar Systems for Object-Based Vegetation Mapping

For this study a framework was designed to effectively combine two datasets (hyperspectral and lidar) and four data processing techniques (data fusion, OBIA, machine learning, and ensemble analysis) for vegetation mapping (Figure 2). In the framework, after the preprocessing of hyperspectral imagery,

the MNF transformed data were first segmented to generate image objects and extract spectral/spatial features, and then the extracted spectral/spatial features were combined with the lidar derived elevation, intensity, and topographic features at the object level to generate a fused dataset. Three machine learning algorithms (RF, SVM, and *k*-NN) were used to pre-classify the fused data. The final outcome was derived through ensemble analysis of the three classification results. Consequently, an object-based vegetation map was generated and evaluated using common accuracy assessment approaches.

Image Segmentation

Image segmentation was a major procedure in OBIA techniques. The multiresolution segmentation algorithm in eCognition® Developer 8.64.1 (Trimble, 2011) was used to generate image objects from the MNF transformed imagery. The segmentation algorithm starts with one-pixel image segments, and merges neighboring segments together until a heterogeneity threshold is reached (Benz *et al.*, 2004). The heterogeneity threshold is determined by a user-defined scale parameter, as

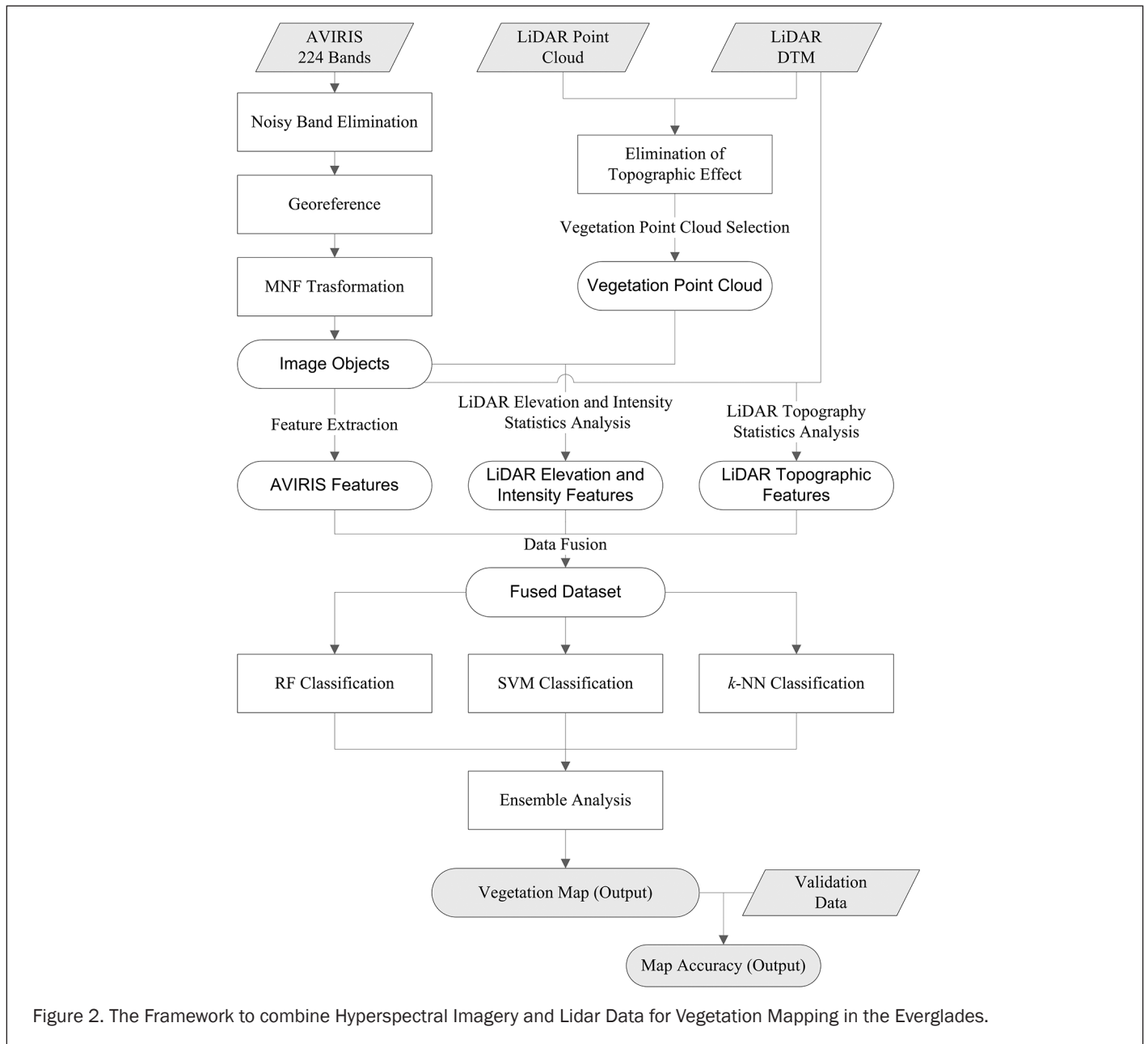


Figure 2. The Framework to combine Hyperspectral Imagery and Lidar Data for Vegetation Mapping in the Everglades.

well as color/shape and smoothness/compactness weights. The image segmentation is scale-dependent, and the quality of segmentation and overall classification depend on the segmentation scale. In order to find an optimal scale for image segmentation, an unsupervised image segmentation evaluation approach (Johnson and Xie, 2011) was used. This approach begins with a series of segmentations using different scale parameters, and then identifies the optimal image segmentation using an unsupervised evaluation method that takes into account global intra-segment and inter-segment heterogeneity measures. A global score (GS) is calculated by $GS = V_{norm} + MI_{norm}$, where V_{norm} (normalized weighted variance) measures the global intra-segment goodness, and MI_{norm} (normalized Moran's I) measures the global inter-segment goodness. More details in computing V_{norm} and MI_{norm} can be found in Johnson and Xie (2011). The GSs are used to determine the optimal scale for segmentation. For the study area the scale parameter of 8 produced the lowest GS value among a series of segmentations with different scale parameters and thus was used here. The weights of the MNF layers were set based on their eigenvalues (66.2, 48.7, 32.4, 17.1, 15.1, 6.4, 4.8, 3.8, 3.7, and 3.6). Color and shape weights were set to 0.9 and 1.0 so that spectral information would be considered more heavily for segmentation. Smoothness and compactness weights were both set to 0.5 so that neither compact nor non-compact segments were favored. Following the segmentation spectral/spatial features (mean and standard deviations) of each object were extracted for further analysis.

Lidar Feature Extraction

Three types of features can be extracted from lidar data: elevation, intensity, and topography. Most studies only examined the contribution of elevation information on vegetation discrimination when lidar was combined with hyperspectral imagery (e.g., Mundt *et al.*, 2006; Jones *et al.*, 2010; Onojeghuo and Blackburn, 2011; Cho *et al.*, 2012). Evaluation of intensity and topography has been limited. Fusion of lidar data and optical imagery can occur at two levels: pixel- and feature-level. Pixel-level fusion combines raw data from multiple sources into single resolution data to improve the performance of image processing tasks. Feature-level fusion extracts features (e.g., edges, corners, lines, and textures) from each individual data source and merges these features into one or more feature maps for further processing.

Previous studies have primarily adopted the pixel-level fusion strategy to combine lidar and hyperspectral imagery (e.g., Jones *et al.*, 2010; Onojeghuo and Blackburn, 2011; Cho *et al.*, 2012). The pixel-level fusion methods commonly begin with the generation of a related raster layer (e.g., digital canopy model) from lidar point cloud data using interpolation techniques, and then combine this raster layer with the co-registered hyperspectral imagery pixel by pixel. This is referred to as the raster-based lidar approach. A major problem using lidar in this way is the introduction of errors and uncertainties in the raster layer generation step, which will ultimately affect the subsequent vegetation delineation (Zhang and Qiu, 2012). To overcome this problem lidar elevation and intensity information was extracted from the original point cloud data rather than the lidar-derived raster layers (Figure 2). This is referred to as the vector-based lidar approach. Studies have proved that working directly on lidar point cloud data can produce higher accuracy by preserving the original lidar values (Zhang and Qiu, 2012).

To effectively use elevation information, topographic effect was eliminated first by subtracting DTM value underneath each lidar point from the elevation. Points with an elevation less than 0.15 meters were considered as ground points to be dropped from further analysis. Non-ground lidar points (vegetation points) within an image object were used to derive the

descriptive statistics (maximum, mean, and standard deviation) of elevation and intensity for this object, respectively. Similarly, descriptive statistics of terrain elevation and slope for each image object were derived from the DTM using pixels within an object (Figure 2). Feature-level fusion strategy was employed to merge the lidar-derived features and hyperspectral-derived measures to be used for classification.

Classification Algorithms: RF, SVM, and k -NN

RF, SVM, and k -NN algorithms were employed to pre-classify the fused dataset. RF is a decision tree-based ensemble classifier. To understand this algorithm, it is helpful to first know the decision tree approach. The decision tree splits training samples into smaller subdivisions at "nodes" using decision rules. For each node, tests are performed on the training data to find the most useful variables and variable values for each split. Different algorithms can be used to generate the decision trees. The RF often adopts the Gini Index to measure the best split selection. More descriptions of RF can be found in Breiman (2001) and in a remote sensing context by Chan and Paelinckx (2008). Two parameters need to be defined in RF: the number of decision trees to create (k) and the number of randomly selected variables (m) considered for splitting each node in a tree. RF is not sensitive to m and it is often blindly set to \sqrt{M} (Gislason *et al.*, 2006). The computational complexity of the algorithm can be reduced by selecting a smaller m ; k is often set based on trial and error.

SVM is a non-parametric supervised machine learning classifier. The aim of SVM is to find a hyperplane that can separate the input dataset into a discrete predefined number of classes in a fashion consistent with the training samples (Vapnik, 1995). SVM research in remote sensing has increased in the past decade, as evidenced by a review in Mountrakis *et al.* (2010). Detailed descriptions of SVM algorithms were given by Huang *et al.* (2002) in the context of remote sensing. Kernel-based SVMs are commonly used in classification, among which the radial basis function (RBF), and the polynomial kernels are frequently employed. RBF needs to set the kernel width (γ), and polynomial kernel needs to set the degree (p). Both kernels need to define a penalty parameter (C) that controls the degree of acceptable misclassification. The setting of these parameters can be determined by a grid search strategy which tests possible combinations of them in a user-defined range (Hsu *et al.*, 2010). Both kernels were tested to find the best model for the fused dataset.

k -NN is another supervised classifier which identifies objects based on the closest training samples in the feature space. It searches away from the unknown object to be classified in all direction until it encounters k user-specified training objects. It then assigns the object to the class with the majority vote of the encountered objects. The algorithm requires all the training data participate in each classification, thus has a slow speed of execution for pixel-based classification (Hardin, 1994). However, for the object-based classification used in this study image objects are minimum classification units, i.e., classification primitives, instead of individual pixels. The amount of classification primitives is greatly reduced through the segmentation process. Therefore computation complexity is not a problem for implementing this algorithm.

Ensemble Analysis

The final classification was derived through an ensemble analysis of the outputs from RF, SVM, and k -NN. An ensemble analysis approach is a multiple classification system that combines the outputs of several classifiers. The classifiers in the system should generally produce accurate results but show some differences in classification accuracy (Du *et al.*, 2012). A range of strategies has been developed to combine the outputs from multiple classifiers, such as the majority

vote, Bayesian average method, and fuzzy integral approach. Among these strategies, the majority vote (each individual classifier votes for an unknown input object) is straightforward. A key problem of the majority vote is that all the classifiers have equal rights to vote without considering their performances on each individual class. A weighting strategy may mitigate this problem by weighting the decision from each classifier based on their accuracies obtained from the reference data (Moreno-Seco *et al.*, 2006). In the framework, the majority vote and the weighting strategy is combined to analyze the outputs from three classifiers. If three votes are different, then the unknown object will be assigned to the class which has the highest accuracy among the classifiers. That is, the classifier with the best performance among three votes will obtain a weight of 1, while weights of the other two classifiers will be set at 0. If two or three classifiers vote the same class for an input object, then the object will be assigned to the same voted class.

Accuracy Assessment

The error matrix and Kappa statistic (Congalton and Green, 2009) has served as the standard approach in accuracy assessment. An error matrix was constructed for the final classified map and the Kappa statistics were calculated. The error matrix can be summarized as an overall accuracy and Kappa value. The overall accuracy is defined as the ratio of the number of validation samples that are classified correctly to the total number of validation samples irrespective of the class. The Kappa value describes the proportion of correctly classified

validation samples after random agreement is removed. To evaluate the statistical significance of differences in accuracy between different classifications, the nonparametric McNemar test (Foody, 2004) was adopted. The difference in accuracy of a pair of classifications is viewed as being statistically significant at a confidence of 95 percent if the z-score is larger than 1.96.

Results

Evaluation of Data Fusion For Vegetation Mapping

Five experiments were designed to evaluate the framework. Experiment 1 used the AVIRIS data alone, and Experiments 2, 3, and 4 combined AVIRIS-derived features with lidar-derived elevation, intensity, and topography information, respectively. Experiment 5 integrated AVIRIS- and all lidar-derived features. The RF classifier was applied first in five experiments. The number of randomly selected variables for splitting node (m) in RF was set to 4 after several trials. A number of tests using different numbers of trees (50 to 300 at an interval of 50) revealed that $k = 150$ resulted in the highest accuracy. The overall accuracies and Kappa values from these experiments are shown in Table 1.

AVIRIS data (Experiment 1) produced an encouraging result with an overall accuracy of 76 percent and a Kappa value of 0.70. Combining AVIRIS with lidar-derived elevation (Experiment 2), intensity (Experiment 3), and topography information (Experiment 4), increased the overall accuracy to 81 percent, 80 percent, and 83 percent, respectively. Kappa values also

TABLE 1. CLASSIFICATION RESULTS FROM DIFFERENT EXPERIMENTS

Classification Accuracies								
Experiment #	1	2	3	4	5	6	7	8
Overall Accuracy	76%	81%	80%	83%	86%	85%	83%	86%
Kappa Value	0.70	0.76	0.75	0.79	0.83	0.81	0.79	0.82
McNemar Tests								
Z-score Value	NA	2.5* (1/2)	2.3* (1/3)	3.3* (1/4)	4.5* (1/5)	0.6 (5/6)	1.8 (5/7)	0.6 (5/8)
		NA	0.3 (2/3)	1.0 (2/4)	3.0* (2/5)	NA	0.9 (6/7)	0.4 (6/8)
			NA	1.3 (3/4)	2.8* (3/5)	NA	NA	1.9 (7/8)
				NA	2.0* (4/5)	NA	NA	NA

Experiments 1-5 used AVIRIS, AVIRIS and lidar-derived elevation, AVIRIS and lidar-derived intensity, AVIRIS and lidar-derived topographic information, and AVIRIS and all lidar-derived features (elevation, intensity, and topographic information), respectively. The Random Forest (RF) classifier was applied in the above five experiments. Experiments 6-8 used a combined dataset of AVIRIS and all lidar-derived features as experiment 5, but applied Support Vector Machine (SVM), k -Nearest Neighbor (k -NN), and ensemble analysis of three classifiers, respectively. For McNemar tests, 1/2, 1/3...7/8 refer to the test between experiments 1 and 2, 1 and 3, ... 7 and 8 respectively.

*: significant with 95 percent confidence.

TABLE 2. PER-CLASS ACCURACIES DERIVED FROM A COMBINED DATASET OF HYPERSPECTRAL IMAGERY AND ALL LIDAR-DERIVED FEATURES USING THREE DIFFERENT CLASSIFIERS (RF, SVM, AND k -NN); THE HIGHEST ACCURACY AMONG THREE CLASSIFIERS IS HIGHLIGHTED IN BOLD

Class	Producer's Accuracy (%)			User's Accuracy (%)		
	RF	SVM	k -NN	RF	SVM	k -NN
1. Unimproved Pasture	72.7	90.9	72.7	80.0	76.9	80.0
2. Upland Shrub and Brushland	72.7	81.8	72.7	66.7	47.4	44.4
3. Mixed Rangeland	82.4	58.8	88.2	60.9	71.4	57.7
4. Upland Hardwood	100.0	100.0	100.0	100.0	100.0	100.0
5. Brazilian Pepper	44.4	44.4	55.6	66.7	66.7	55.6
6. Live Oak	85.7	78.6	71.4	85.7	73.3	83.3
7. Upland Mixed Coniferous/Hardwood	79.2	70.8	58.3	70.4	77.3	66.7
8. Mixed Shrub	82.4	88.2	76.5	93.3	93.8	81.3
9. Freshwater Marshes/Graminoid Prairie-Marsh	98.3	97.4	97.4	94.2	95.7	94.9
10. Wet Prairie	70.0	50.0	30.0	87.5	55.6	100.0
11. Emergent Aquatic Vegetation	91.7	88.9	91.7	94.3	94.1	91.7
12. Sugar Cane	88.9	88.9	88.9	100.0	100.0	100.0
13. Herbaceous (Dry Prairie)	58.3	66.7	66.7	87.5	80.0	88.9

showed corresponding improvements. McNemar tests showed that these improvements were statistically significant. Integration of AVIRIS-derived measures and all lidar-derived features (Experiment 5) generated the best result with an overall accuracy of 86 percent and a Kappa value of 0.83. McNemar tests showed that Experiment 5 generated significantly better outcome than Experiments 1 through 4 (Table 1). Experiments 2, 3, and 4 showed no significant difference in classification.

Evaluation of Different Classifiers and Ensemble Analysis for Vegetation Mapping
 Experiment 5 achieved the best result, thus the SVM and k -NN classifiers were applied first to the fully fused dataset as Experiment 5 to explore their performances. For the SVM algorithms, after a number of trials using polynomial and RBF kernels, the polynomial kernel with the degree parameter (p) set to 2, and penalty error parameter (C) set to 2.0 generated the best result. For the k -NN method, k was specified to 3 after several trials. The results are listed in Table 1 as Experiments 6 (SVM) and 7 (k -NN). SVM produced a comparable accuracy (85 percent) with the RF classifier, while k -NN generated the lowest accuracy (83 percent) among them. The McNemar tests revealed that there was no significant difference in classification among three classifiers. The SVM and k -NN approaches were also tested to other datasets used in Experiments 1 through 4 and the results supported the findings here, i.e., no significant difference among three classifiers in classifying each dataset.

The per-class accuracies from Experiments 5, 6, and 7 are shown in Table 2. The performances of three classifiers were not completely even in identifying each class. For example, from the producer's perspective, RF produced the best result in characterizing classes 6, 7, 9, and 10; SVM had the best performance in discriminating classes 1, 2, and 8; and k -NN showed the highest accuracy in classifying classes 3 and 5. From the user's perspective, RF was the best in discriminating classes 2, 6, and 11; SVM was the best in identifying 3, 7, 8, and 9; and k -NN produced the highest accuracy for classes 10, and 13. This diversity is primarily caused by the discrepancies in concepts of three methods. RF looks for optimal decision trees to group data, whereas SVM looks for the optimal

hyperplane to categorize data and k -NN searches for the best match to denote inputs. The diversity drives the exploration of the ensemble analysis. The difference in outputs from multiple classifiers is an assumption of classifier ensemble techniques. The ensemble analysis result is displayed as Experiment 8 in Table 1. A total accuracy of 86 percent and a Kappa value of 0.82 were obtained, showing no large improvement in the classification accuracy. McNemar test also illustrated there were no significant differences in classification between the ensemble analysis and each individual classifier involved in the ensemble.

Object-based Vegetation Mapping

Landis and Koch (1977) suggested that Kappa values larger than 0.81 indicate an almost perfect agreement. The designed framework produced an overall accuracy of 86 percent with a Kappa value of 0.82 based on the calibration data, indicating it is effective for vegetation mapping. An object-based vegetation map was thus produced using the fused dataset and ensemble analysis, as shown in Plate 1a. The object-based vegetation map is more informative and useful than a traditional pixel-based one that may be noisy if the study area has a high degree of spatial and spectral heterogeneity. The error matrix for the classified map is displayed in Table 3. The producer's accuracies (PA) changed from 40.0 percent (*Wet Prairie*) to 100.0 percent (*Upland Hardwood*) and the user's accuracies (UA) varied from 53.3 percent (*Upland Shrub and Brushland*) to 100.0 percent (*Upland Hardwood*). *Wet Prairie* is one of the most diverse communities in the Everglades. It is a mixture of water, marshes, algal plants, and a variety of vascular plants. A low accuracy is expected in identifying this community.

Although ensemble analysis did not improve the classification accuracy, it can make the result more reliable. In addition, ensemble analysis can provide some complementary information to the error matrix of the classified map. An uncertainty map can be derived based on the ensemble analysis, as shown in Plate 1b. If three votes are the same for an input image object, a complete agreement will be achieved. Conversely, if three votes are completely different, no agreement

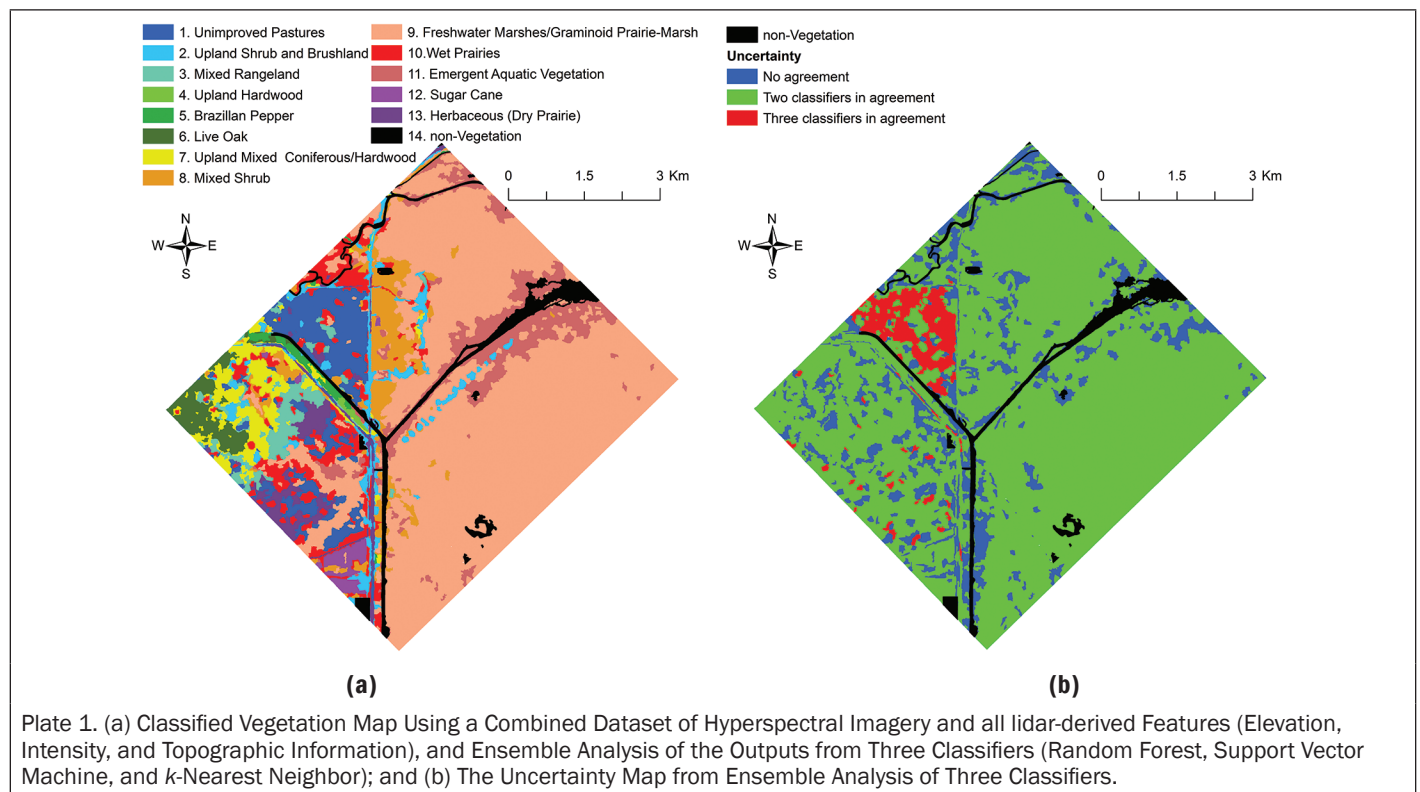


TABLE 3. ERROR MATRIX FOR THE FINAL CLASSIFIED MAP THAT WAS PRODUCED USING A SYNERGY OF HYPERSPECTRAL IMAGERY AND ALL LIDAR-DERIVED FEATURES, AND ENSEMBLE ANALYSIS OF THE OUTPUTS FROM RANDOM FOREST (RF), SUPPORT VECTOR MACHINE (SVM), AND *k*-NEAREST NEIGHBOR (*k*-NN) CLASSIFIERS (EXPERIMENT 8 IN TABLE 1); THE NAME OF CLASSES 1 THROUGH 13 IS LISTED IN TABLE 2

Class #	1	2	3	4	5	6	7	8	9	10	11	12	13	Row Total	PA (%)
1	16		3				1		1	1				22	72.7
2	1	8	1				1							11	72.7
3		1	15										1	17	88.2
4				2										2	100.0
5		1			4	1	3							9	44.4
6					2	11	1							14	78.6
7			5			2	17							24	70.8
8		1						15	1					17	88.2
9									113		2			115	98.3
10	1	1	1					1	2	4				10	40.0
11									2		34			36	94.4
12		1										8		9	88.9
13	2	2											8	12	66.7
Col. Total	20	15	25	2	6	14	23	16	119	5	36	8	9	Overall accuracy: 86%	
UA (%)	80.0	53.3	60.0	100.0	66.7	78.6	73.9	93.8	95.0	80.0	94.4	100.0	88.9	Kappa value: 0.82	

UA: User's Accuracy; PA: Producer's Accuracy; Classification result is displayed in row, and the reference data is displayed in column.

will be obtained. If only two classifiers vote for the same class, a partial agreement will be produced. A joint analysis of the classified vegetation map and uncertainty map revealed that the dominant community (class 9: freshwater marshes/graminoid prairie-marsh) was mainly voted by two classifiers. A further examination showed that this class was mainly voted by RF and SVM, while *k*-NN voted it as other communities. This type of uncertainty map is useful when there is a desire to minimize the omission or commission errors. It also can be used to guide the post-classification fieldwork (Foody *et al.*, 2007). To the best of my knowledge, no such uncertainty map has been published based on the classifier ensemble analysis. Further research is needed to investigate the potential application of this type of map in remote sensing.

Discussion

Previous studies have demonstrated that multispectral systems cannot accurately map the diverse vegetation communities in the Everglades (Zhang and Xie, 2013b; Zhang *et al.*, 2013). With the emergence of hyperspectral techniques, it is anticipated that the manual interpretation of aerial photograph procedure currently used in CERP can be superseded by an automated procedure. However, exploration of hyperspectral techniques for plant study in the complex wetlands is not simple. Hirano *et al.* (2003) reported a moderate accuracy for mapping vegetation over a portion of the coastal Everglades (i.e., 66 percent). This moderate accuracy was mainly caused by the inadequate spatial resolution (20 meters) and their limited examination of hyperspectral data analysis techniques. To enhance the application of hyperspectral systems in the Florida Everglades, the author's research group has conducted a few studies to investigate what detail level and accuracy can be obtained using different types of hyperspectral imagery and data fusion techniques (Zhang and Xie, 2012; Zhang and Xie, 2013a and 2013b). Two types of hyperspectral imagery were available for these studies and collected at different regions in the Everglades: very high spatial resolution data (i.e., 5 meters or smaller), and high spatial resolution data (10 to 30 meters). In Zhang and Xie (2012) 4-meter AVIRIS imagery was used to map 12 vegetation communities in the central

Everglades. A neural network based classifier was developed and spatial information derived from texture analysis was examined and proved useful. In Zhang and Xie (2013a), 3.5-meter HyMap imagery was used to map 14 vegetation communities and 55 species using hierarchical segmentation techniques in the northern Everglades. These two Studies (Zhang and Xie, 2012 and 2013a) have found that very high spatial resolution hyperspectral data are able to generate good results (>80 percent in accuracy), but collection of this type of data is costly. It is impractical to use this type of data for a broad area mapping in CERP.

In contrast, Zhang and Xie (2013b) have evaluated the applicability of 20-meter hyperspectral imagery for vegetation mapping in the Everglades. They have found that this type of hyperspectral imagery alone cannot classify spectrally mixed objects as well as map communities present as small patches or linear/narrow shapes. To mitigate this problem they fused 20-meter hyperspectral imagery and 1-meter digital aerial photography and developed a pixel/feature-level fusion strategy. The fused data were then used to map vegetation in the same study area as Hirano *et al.* (2003). An overall accuracy of 90 percent was obtained, suggesting data fusion is an effective solution. But data should be collected simultaneously to avoid the temporal changes. Zhang *et al.* (2013) examined a combination of lidar and digital aerial photography for Everglades mapping because aerial photographs are frequently collected in CERP. Application of 1-meter digital aerial photography (four bands) alone produced an overall accuracy of 49 percent in mapping seven forest communities. When lidar was fused with the aerial photography, a moderate accuracy was obtained (71 percent).

To improve the application of data fusion techniques in the Everglades, in this study 12-meter hyperspectral imagery was fused with lidar data at the object level. An encouraging accuracy (76 percent) was obtained using 12-meter hyperspectral data alone, indicating spectral resolution is more important than spatial resolution. This accuracy was increased to 86 percent when hyperspectral imagery was combined with lidar data. Accurate and automated identification of vegetation communities in the Everglades is a difficult task because most communities are a mixture of trees, shrub/scrub, herbaceous

ground plants, water, and bare soil. This study illustrates that a synergy of hyperspectral and lidar systems is effective for mapping the diverse vegetation communities in the Everglades. Inclusion of lidar-derived features (elevation, intensity, and topography) significantly increased the classification accuracy, showing the promise of modern hyperspectral and lidar systems in the Everglades mapping. Note that there was a 5.5-year time gap between acquisition of AVIRIS data (May 2002) and lidar data (December 2007). Topographic features might have not changed too much in 5.5 years, but vegetation structure characterized by lidar might have been severely changed. Simultaneous collection of two data sources may be able to produce higher accuracy. In addition, increasing the lidar point density may help improve the classification accuracy by better characterizing the vegetation structure.

Lidar elevation was believed to be the most useful information in vegetation classification, and thus has been commonly combined with optical imagery to improve mapping results (Jones *et al.*, 2010; Cho *et al.*, 2012). The study confirms the gain from lidar elevation in vegetation mapping. Little work has been published on the information content of the lidar intensity returns for vegetation analysis. There are three major factors affecting lidar intensity: the illuminated area, bidirectional reflectance distribution function of the illuminated targets, and incidence angles. This means radiometric lidar features will exhibit substantial variation due to differences in the illuminated area (foliage density), reflectance of illuminated scatters, and the geometry of leaf scatters (leaf orientation) (Korpela *et al.*, 2010). Therefore application of lidar intensity needs to be based on the analysis of distribution characteristics, rather than each single pulse. Moffiet *et al.* (2005) indicated that lidar intensity statistics may be useful variables to assist with forest discrimination based on their data exploration analysis. But this has not been proven in practice or research. Chust *et al.* (2008) found that a filtered lidar intensity image can improve classification accuracy, while the raw intensity image contributes nothing for the habitat mapping in a coastal wetland. This study illustrates the benefit of lidar intensity statistics to vegetation mapping. Topographic information also increased the classification accuracy, which is consistent with the results reported by Chust *et al.* (2008) in wetland habitat mapping and Ke *et al.* (2010) in forest mapping. Topographic features are usually homogeneous within an object, which can help reduce the within-class variability among neighboring objects caused by shadows or gaps thus increasing the classification accuracy. In this study the intensity and topographic features made similar contributions as to the elevation information.

As mentioned in the Methodology Section, various dimensionality reduction algorithms have been developed in hyperspectral data preprocessing. It will be interesting to evaluate the impacts of different algorithms on the classification accuracy. It is also worth to determine the best hyperspectral narrowbands (HNBs) and/or hyperspectral vegetation indices (HVIs) in identifying each community as well as to assess the classification accuracies achievable using various combinations of the best HNBs and HVIs. Combining more data sources in the mapping procedure is also attractive. Note that several parameters need to be specified for each classifier used in this study. The setting of these parameters may be site specific and training/testing data sensitive. So far most researchers set these parameters based on empirical tests. Automated searching within a user-defined range as Hsu *et al.* (2010) proposed for the SVM algorithm may be a good solution to other classifiers. These will be major dedications in the future work. It is anticipated that this study can enhance the application of hyperspectral and lidar systems in complex wetland mapping.

Summary and Conclusions

In this study an integration of hyperspectral and lidar systems for vegetation mapping in the Florida Everglades was examined. To effectively apply two data sources in the mapping procedure, a framework was designed to integrate Object-Based Image Analysis (OBIA), machine learning algorithms, and ensemble analysis techniques. The following conclusions were drawn from this study:

1. Hyperspectral systems are promising for vegetation mapping in the Florida Everglades. Application of high spatial resolution hyperspectral imagery (12 meters) produced an overall accuracy of 76 percent and a Kappa value of 0.70 in discriminating 13 vegetation communities.
2. Low-posting-density lidar data are useful in the Florida Everglades. An integration of all lidar-derived features (elevation, intensity, and topographic information) and hyperspectral data achieved an overall accuracy of 86 percent with a Kappa value of 0.82. Lidar elevation, intensity, and topography made the same contribution to the classification.
3. Three machine learning algorithms (Random Forest (RF), Support Vector Machine (SVM), and *k*-Nearest Neighbor (*k*-NN)) are valuable in processing the fused hyperspectral and lidar data. All of them performed well in the classification. An ensemble analysis of the outputs from three classifiers did not improve the classification accuracy, but it provided a supplementary uncertainty map to assist with the traditional error matrix in accuracy assessment.
4. An integration of hyperspectral and lidar data shows potential to map diverse vegetation communities in complex wetlands. The designed framework can be used as an alternative to the current manual interpretation procedure for updating and building vegetation databases in the Florida Everglades. With the increasing availability of two types of data it is anticipated that this study can benefit the global wetland mapping in general, and the Florida Everglades in particular.

Acknowledgments

Dr. Zhixiao Xie assisted with the image segmentation. Dr. Prasad S. Thenkabil provided valuable comments and suggestions, which improved an earlier version of this paper.

References

- Adam, E., O. Mutanga, and D. Rugege, 2010. Multispectral and hyperspectral remote sensing for identification and mapping of wetland vegetation: A review, *Wetlands Ecology and Management*, 18:281–296.
- Addink, E.A., S.M. de Jong, and E.J. Pebesma, 2007. The importance of scale in object-based mapping of vegetation parameters with hyperspectral imagery, *Photogrammetric Engineering & Remote Sensing*, 73(9):905–912.
- Artigas, F.J., and J.S. Yang, 2005. Hyperspectral remote sensing of marsh species and plant vigour gradient in the New Jersey Meadowlands, *International Journal of Remote Sensing*, 26:5209–5220.
- Belluco, E., M. Camuffo, S. Ferrari, L. Modenese, S. Silvestri, A. Marani, and M. Marani, 2006. Mapping salt-marsh vegetation by multispectral and hyperspectral remote sensing, *Remote Sensing of Environment*, 105:54–67.
- Benz, U., P. Hofmann, G. Willhauck, I. Lingenfelder, and M. Heynen, 2004. Multiresolution, object-oriented fuzzy analysis of remote sensing data for GIS-ready information, *ISPRS Journal of Photogrammetry and Remote Sensing*, 58:239–258.
- Blaschke, T., 2010. Object based image analysis for remote sensing, *ISPRS Journal of Photogrammetry and Remote Sensing*, 65:2–16.
- Breiman, L., 2001. Random forests, *Machine Learning*, 45: 5–32.

- Chan, J.C.-W., and D. Paelinckx, 2008. Evaluation of Random Forest and Adaboost tree based ensemble classification and spectral band selection for ecotope mapping using airborne hyperspectral imagery, *Remote Sensing of Environment*, 112:2999–3011.
- Cho, M.A., R. Mathieu, G.P. Asner, L. Naidoo, J. van Aardt, A. Ramoelo, P. Debba, K. Wessels, R. Main, I.P.J. Smit, and B. Erasmus, 2012. Mapping tree species composition in South African savannas using an integrated airborne spectral and LiDAR system, *Remote Sensing of Environment*, 125:214–226.
- Chust, G., I. Galparsoro, A. Borja, J. Franco, and A. Uriarte, 2008. Coastal and estuarine habitat mapping using LiDAR height and intensity and multispectral imagery, *Estuarine, Coastal and Shelf Science*, 78:633–643.
- Cohen, S., Y. Cohen, V. Alchanatis, and O. Levi, 2013. Combining spectral and spatial information from aerial hyperspectral images for delineating homogenous management zones, *Biosystems Engineering*, 114:435–443.
- Comprehensive Everglades Restoration Plan (CERP), <http://www.evergladesplan.org/> (last date accessed: 02 June 2014).
- Congalton, R., and K. Green, 2009. *Assessing the Accuracy of Remotely Sensed Data: Principles and Practices*, Second edition, CRC/Taylor & Francis, Boca Raton, Florida.
- Davis, S.M., L.H. Gunderson, W.A. Park, J. Richardson, and J. Mattson, 1994. Landscape dimension, composition, and function in a changing Everglades ecosystem, *Everglades: The Ecosystem and its Restoration* (S.M. Davis and J.C. Ogden, editors), St Lucie Press, Delray Beach, Florida, pp. 419–444.
- Doren, R.F., K. Rutchev, and R. Welch, 1999. The Everglades: A perspective on the requirements and applications for vegetation map and database products, *Photogrammetric Engineering & Remote Sensing*, 65(2):155–161.
- Du, P., J. Xia, W. Zhang, K. Tan, Y. Liu, and S. Liu, 2012. Multiple classifier system for remote sensing image classification: A review, *Sensors*, 12:4764–4792.
- Footy, G.M., 2004. Thematic map comparison, evaluating the statistical significance of differences in classification accuracy, *Photogrammetric Engineering & Remote Sensing*, 70(6):627–633.
- Footy, G.M., D.S. Boyd, and C. Sanchez-Hernandez, 2007. Mapping a specific class with an ensemble of classifiers, *International Journal of Remote Sensing*, 28:1733–1746.
- Geerling, G.W., M.Labrador-Garcia, J.G.P. W. Clevers, A.M.J. Ragas, and A.J.M. Smits, 2007. Classification of floodplain vegetation by data fusion of spectral (CASI) and LiDAR data, *International Journal of Remote Sensing*, 28:4263–4284.
- Gislason, P.O., J.A. Benediktsson, and J.R. Sveinsson, 2006. Random Forests for land cover classification, *Pattern Recognition Letters*, 27:294–300.
- Green, A.A., M. Berman, P. Switzer, and M.D. Craig, 1988. A transformation for ordering multispectral data in terms of image quality with implications for noise removal, *IEEE Transactions on Geoscience and Remote Sensing*, 26:65–74.
- Ham, J., Y. Chen, M.M. Crawford, and J. Ghosh, 2005. Investigation of the Random Forest framework for classification of hyperspectral data, *IEEE Transactions on Geoscience and Remote Sensing*, 43:492–501.
- Hardin, P.J., 1994. Parametric and nearest-neighbor methods for hybrid classification: A comparison of pixel assignment accuracy, *Photogrammetric Engineering & Remote Sensing*, 60(12):1439–1448.
- Harken, J., and R. Sugumaran, 2005. Classification of Iowa wetlands using an airborne hyperspectral image: A comparison of the spectral angle mapper classifier and an object-oriented approach, *Canadian Journal of Remote Sensing*, 31:167–174.
- Held, A., C. Ticehurst, L. Lymburner, and N. Williams, 2003. High resolution mapping of tropical mangrove ecosystems using hyperspectral and radar remote sensing, *International Journal of Remote Sensing*, 24:2739–2759.
- Hill, R.A., and A.G. Thomson, 2005. Mapping woodland species composition and structure using airborne spectral and LiDAR data, *International Journal of Remote Sensing*, 26:3763–3779.
- Hirano, A., M. Madden, and R. Welch, 2003. Hyperspectral image data for mapping wetland vegetation, *Wetlands*, 23:436–448.
- Hsu, C., C. Chang, and C. Lin, 2010. *A Practical Guide to Support Vector Classification, Final Report*, National Taiwan University, Taipei City, Taiwan.
- Huang, C., L.S. Davis, and J.R.G. Townshend, 2002. An assessment of support vector machines for land cover classification, *International Journal of Remote Sensing*, 23:725–749.
- Hughes, G.F., 1968. On the mean accuracy of statistical pattern recognizers, *IEEE Transactions on Information Theory*, 14:55–63.
- Hunter, E.L., and C.H. Power, 2002. An assessment of two classification methods for mapping Thames Estuary intertidal habitats using CASI data, *International Journal of Remote Sensing*, 23:2989–3008.
- Hyypä, J., H. Hyypä, D. Leckie, F. Gougeon, X. Yu, and M. Maltamo, 2008. Review of methods of small-footprint airborne laser scanning for extracting forest inventory data in boreal forests, *International Journal of Remote Sensing*, 29:1339–1366.
- Jensen, J.R., 2004. *Introductory Digital Image Processing: A Remote Sensing Perspective*, Third edition, Prentice Hall Series in Geographic Information Science.
- Johnson, B., and Z. Xie, 2011. Unsupervised image segmentation evaluation and refinement using a multi-scale approach, *ISPRS Journal of Photogrammetry and Remote Sensing*, 66:473–483.
- Jollineau, M.Y., and P.J. Howarth, 2008. Mapping an inland wetland complex using hyperspectral imagery, *International Journal of Remote Sensing*, 29:3609–3631.
- Jones, J.W., 2011. Remote sensing of vegetation pattern and condition to monitor changes in Everglades biogeochemistry, *Critical Reviews in Environmental Science and Technology*, 41:64–91.
- Jones, T.G., N.C. Coops, and T. Sharma, 2010. Assessing the utility of airborne hyperspectral and LiDAR data for species distribution mapping in the coastal Pacific Northwest, Canada, *Remote Sensing of Environment*, 114:2841–2852.
- Kamal, M., and S. Phinn, 2011. Hyperspectral data for mangrove species mapping: A comparison of pixel-based and object-based approach, *Remote Sensing*, 3:2222–2242.
- Ke, Y., L.J. Quackenbush, and J. Im, 2010. Synergistic use of QuickBird multispectral imagery and LiDAR data for object-based forest species classification, *Remote Sensing of Environment*, 114:1141–1154.
- Korpela, I., H.O. Ørka, M. Maltamo, T. Tokola, and J. Hyypä, 2010. Tree species classification using airborne LiDAR - Effects of stand and tree parameters, downsizing of training set, intensity normalization, and sensor type, *Silva Fennica*, 44:319–339.
- Landis, J., and G.G. Koch, 1977. The measurement of observer agreement for categorical data, *Biometrics*, 33:159–174.
- Li, L., S.L. Ustin, and M. Lay, 2005. Application of multiple endmember spectral mixture analysis (MESMA) to AVIRIS imagery for coastal salt marsh mapping: A case study in China Camp, CA, USA, *International Journal of Remote Sensing*, 26:5193–5207.
- McPherson, B.F., and R. Halley, 1996. The south Florida environment - A region under stress, *U.S. Geological Survey Circular 1134*.
- Moffiet, T., K. Mengersen, C. Witte, R. King, and R. Denham, 2005. Airborne laser scanning: Exploratory data analysis indicates potential variables for classification of individual trees or forest stands according to species, *ISPRS Journal of Photogrammetry and Remote Sensing*, 59:289–309.
- Moreno-Seco, F., J. Iñesta, P. de León, and L. Micó, 2006. Comparison of classifier fusion methods for classification in pattern recognition tasks, *Proceedings of the Joint IAPR International Conference on Structural, Syntactic, and Statistical Pattern Recognition*, pp. 705–713.
- Mountrakis, G., J. Im, and C. Ogole, 2010. Support vector machines in remote sensing: A review, *ISPRS Journal of Photogrammetry and Remote Sensing*, 66:247–259.
- Mundt, J.T., D.R. Streutker, and N.F. Glenn., 2006. Mapping sagebrush distribution using fusion of hyperspectral and lidar classifications, *Photogrammetric Engineering & Remote Sensing*, 72(1):47–54.
- Onojeghuo, A.O., and G.A. Blackburn, 2011. Optimising the use of hyperspectral and LiDAR data for mapping reedbed habitats, *Remote Sensing of Environment*, 115:2025–2034.

- Pengra, B.W., C.A. Johnston, and T.R. Loveland, 2007. Mapping an invasive plant, *Phragmites australis*, in coastal wetlands using the EO-1 Hyperion hyperspectral sensor, *Remote Sensing of Environment*, 108:74–81.
- Plaza, A., J.A. Benediktsson, J.W. Boardman, J. Brazile, L. Bruzzone, G. Camps-Valls, J. Chanussot, M. Fauvel, P. Gamba, A. Gualtieri, M. Marconcini, J.C. Tilton, and G. Trianni, 2009. Recent advances in techniques for hyperspectral image processing, *Remote Sensing of Environment*, 113:S110–S122.
- Rosso, P.H., S.L. Ustin, and A. Hastings, 2005. Mapping marshland vegetation of San Francisco Bay, California, using hyperspectral data, *International Journal of Remote Sensing*, 26:5169–5191.
- Rutchev, K., T. Schall, and F. Sklar, 2008. Development of vegetation maps for assessing Everglades restoration progress, *Wetlands*, 28:806–816.
- Schmidt, K.S., A.K. Skidmore, E.H. Kloosterman, H. Vanoostern, L. Kumar, and J.A.M. Janssen, 2004. Mapping coastal vegetation using an expert system and hyperspectral imagery, *Photogrammetric Engineering & Remote Sensing*, 70(6):703–715.
- Thenkabail, P.S., E.A. Enclona, M.S. Ashton, and B. Van Der Meer, 2004. Accuracy assessments of hyperspectral waveband performance for vegetation analysis applications, *Remote Sensing of Environment*, 91:354–376.
- Thenkabail, P.S., I. Mariotto, M.K. Gumma, E.M. Middleton, D.R. Landis, and K.F. Huemmrich, 2013. Selection of hyperspectral narrowbands (HNBS) and composition of hyperspectral twoband vegetation indices (HVIs) for biophysical characterization and discrimination of crop types using field reflectance and Hyperion/EO-1 data, *IEEE Journal of Selected Topics in Applied Earth Observations and Remote Sensing*, 6:427–439.
- Thenkabail, P.S., G.J. Lyon, and A. Huete, 2011. *Hyperspectral Remote Sensing of Vegetation*, CRC Press, Boca Raton, Florida.
- Trimble, 2011. *eCognition Developer 8.64.1 Reference Book*.
- Vapnik, V.N., 1995. *The Nature of Statistical Learning Theory*, New York: Springer-Verlag.
- van Leeuwen, M., and M. Nieuwenhuis, 2010. Retrieval of forest structural parameters using LiDAR remote sensing, *European Journal of Forest Research*, 129:749–770.
- Waske, B., J.A. Benediktsson, K. Árnason, and J.R. Sveinsson, 2009. Mapping of hyperspectral AVIRIS data using machine-learning algorithms, *Canadian Journal of Remote Sensing*, 35:S106–S116.
- Webb, A.R., 2002. *Statistical Pattern Recognition*, Second edition, Hoboken, New Jersey, Wiley.
- Welch, R., M. Madden, and R.F. Doren, 1999. Mapping the Everglades, *Photogrammetric Engineering & Remote Sensing*, 65(1):163–170.
- Yang, J., and F.J. Artigas, 2010. Mapping salt marsh vegetation by integrating hyperspectral and LiDAR remote sensing, *Remote Sensing of Coastal Environments* (J. Wang, editor), CRC Press, Boca Raton, Florida, pp. 173–190.
- Zhang, C., and F. Qiu, 2012. Mapping individual tree species in an urban forest using airborne lidar and hyperspectral imagery, *Photogrammetric Engineering & Remote Sensing*, 78(10):1079–1087.
- Zhang, C., and Z. Xie, 2012. Combining object-based texture measures with a neural network for vegetation mapping in the Everglades from hyperspectral imagery, *Remote Sensing of Environment*, 124:310–320.
- Zhang, C., and Z. Xie, 2013a. Object-based vegetation mapping in the Kissimmee River watershed using HyMap data and machine learning techniques, *Wetlands*, 33:233–244.
- Zhang, C., and Z. Xie, 2013b. Data fusion and classifier ensemble techniques for vegetation mapping in the coastal Everglades, *Geocarto International*, doi: 10.1080/10106049.2012.756940.
- Zhang, C., Z. Xie, and D. Selch, 2013. Fusing LiDAR and digital aerial photography for object-based forest mapping in the Florida Everglades, *GIScience & Remote Sensing*, 50:562–573.
- Zhang, L., Y. Zhong, B. Huang, J. Gong, and P. Li, 2007. Dimensionality reduction based on clonal selection for hyperspectral imagery, *IEEE Transactions on Geoscience and Remote Sensing*, 45:4172–4186.